ETH
Eidgenössische Technische Hochschule Zürich
Swiss Federal Institute of Technology Zurich

HARVARD
UNIVERSITY

Development and evaluation of a soft underwater Robot

Master Thesis

Robert Hennig

Cambridge, MA, August 24, 2020

Supervisors:
Prof. Dr. Conor Walsh Visor, Alex Beaudette
Harvard Biodesign Lab

Tutor:
Janos Vörös,
ETH Zürich

Abstract

Soft underwater robotics have gained attention for scientific study of marine life, replicating natural swimming behaviours, providing a platform for swarm analysis and many other applications. However, current technologies for soft underwater robots show a big trade off between simplicity and functionality.

The master thesis presents the design, development and implementation of a novel magnetic actuation technique which is inherently simple, modular and swift. Repulsive and attractive forces between an electromagnet and permanent magnet, which is embedded in a soft structure, are exploited. This causes a deformation of the soft structure. In this case a bend of a silicon cast tail with optimised shape and flexibility. Upon cyclic repetition, an undulating motion is generated actuating the underwater robot. This swimming behaviour is inspired by thunniform propulsion found in nature. All the components were integrated into a mermaid shaped body with full water protection of all electric and mechanical parts. A series of swimming tests confirmed the ability to swim untethered at a velocity of 10.8 cm/s.

The established prototype exemplifies the realisation of the novel actuation principle. The new modular and straightforward setup makes it appropriate for education and research with great potential for further optimisation and extension. This new generation of soft robotic actuation has large potential in other applications providing immediate control and direct output in a transmission free setup.

Acknowledgements

I would like to express my sincere gratitude to Prof. Conor Walsh for giving me the opportunity to do my master's thesis in the Harvard Biodesign Lab and the insightful guidance throughout the project. I would like give a big thank you to my supervisor Alex Beaudette, for the great support throughout the project while giving me the freedom and independence to grow as an engineer and scientist. Besides my supervisors, I would like to thank my tutor from ETH Zurich, Prof. Janos Vörös, for all his help with the organisation of the master thesis. I would like to thank Lana Wagner for her help designing the custom PCB and looking into image processing to detect objects underwater.

A big thank you to Derek Cascio, who contributed with great design ideas of the overall body and illustrations. A special thanks goes to Daniel Vogt and Micheal Bell from the Harvard Microrobotics Lab for helping me with all my questions about soft robotics and introducing me to the injection molding process. I would like to thank Florian Berlinger for his advice on underwater robots and Dmitry Popov for introducing me to the Instron testing machine. As a significant part of the thesis was done remotely from home due to the COVID-19 pandemic I would like to thank my roommate Tamara Traitteur for the mental, moral and food support and helping with illustrations.

Contents

Chapter 1

Introduction

1.1 Objective

This master thesis aims to develop and evaluate a soft underwater robot. An effort by my supervisor, Prof. Conor Walsh is the soft robotics toolkit, a website enabling students from primary school do graduate students to learn about soft robotics. The longterm goal is to integrate this robot into a workshop that will fascinate students about soft underwater robots. Goals which the underwater robot should ideally fulfil were established.

- Fin for propulsion. Inspired by nature, the caudal (rear) fin should be actuated to propel the underwater robot forward like a fish.
- Simple, modular and robust design. The design should have a very low complexity while retaining functionality and versatility. Using a low number of simple components allows the robot to be used by students and makes the design inherently robust. Additionally it makes it cost effective.
- Depict a character. To appeal to younger students the outer shape should be humanoid while allowing some flexibility in proportions. Inspiration can be taken from superhero comic characters like mermaids.
- Soft robotics education. The robot should have features that demonstrate the use case of soft robotics, therefore teaching it in a practical hands on experience.
- Real world purpose. One goal is to demonstrate an application for such an underwater robot.

The project was approached in multiple phases. First, a concept was developed. Here the state of the art (Chapter 1.2) was investigated which lead to coming up with a unique approach (Chapter 1.3). Next, in particular the

actuation method was verified for its feasibility (Chapter 2). Upon ensuring the functionality of the approach the whole underwater robot including body, electronics, actuation method and fin was implemented. Tests, simulations and investigating theory lead to improvements and a new iteration of implementation. This cycle was repeated numerous times and the final underwater robot along with the learnings along the way are presented in this report. In the end an outlook is given on possible ways of continuing the project.

1.2 State of the Art

1.2.1 Soft Robotics Overview

While rigid robotics excel in controlled environments, animals and humans often serve as the benchmark when it comes to real world applications [22]. Out of an urge to replicate more natural systems, a new field of soft robotics has emerged. Soft by definition is not only bendable, but also stretchable movements enabling not only new possibilities, but also posing difficult challenges for the design and development. On the one hand, precise manipulation and control becomes more challenging compared to rigid robotics, where strong and precise actuators are established and their simulation is linear and therefore straight forward. On the other hand, by using compliant systems, one can utilise a lot of techniques found in the natural world. One example is the achievement of dynamic gaits like humans, by storing elastic energy in compliant bones and soft tissue. [22] Another example are insect like robots, replicating flying and walking movement [14, 15]. Soft robotics have great potential regarding new actuation and sensing methods and can benefit significantly from bioinspired solutions. While there are many well investigated low cost actuation methods, achieving complex motion is challenging. This is due to the usually one dimensionality of soft actuators, meaning they either bend, jump, twist, extend or flex only enabling a very niche application [19, 2, 12]. To achieve complex motion like a heart contraction multiple actuators need to work synergistically and be arranged in a well designed and thought out way (compare [21]).

A compliant design can create robots, that interact with the environment, humans and animals in a completely new way. One benefit is that they are inherently safe, as even a false actuation does not result in eg. a rigid metal arm hitting a person. Large and rigid robots currently used in e.g. car manufacturing are usually completely encapsulated to avoid accidents with humans. In the future, soft robots can work hand in hand with humans. Additionally there are not only the benefits of the replicated natural system, but by applying the same mechanism the robot fits into nature creating less disruption. This not only seems more appealing to humans, but enables e.g.

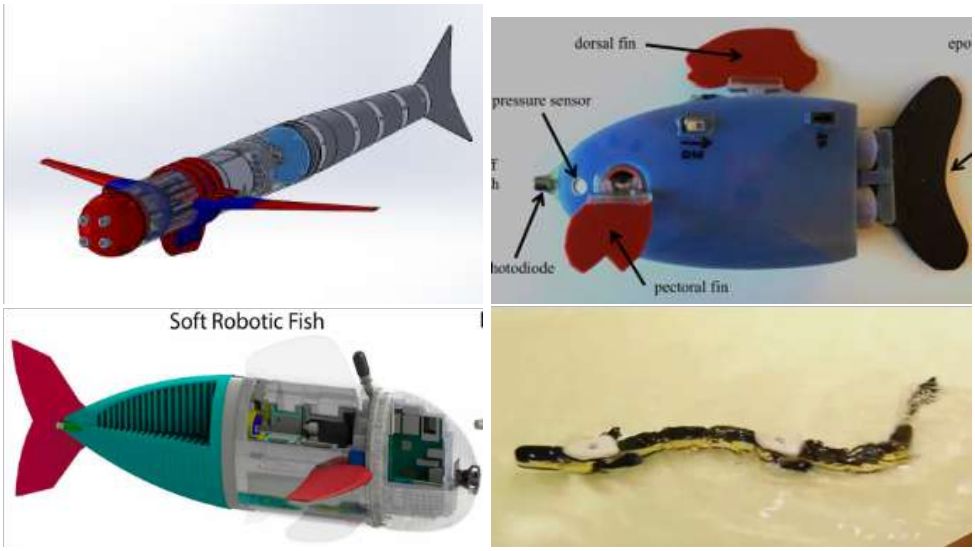

Figure 1.1: (top left) a glider robot, actuated using strings; (top right) a miniature robot for swarm simulation utilising magnetic in coil actuation; (bottom left) an advanced robotic fish using pneumatic actuation; (bottom right) a salamander inspired robot using hinge joints to recreate a undulating spinal cord model

wildlife observation [17] or integration into natural systems like medical assistive devices [23]. New insights to the underwater world can be gained by close non-disruptive observations replicating fish locomotion with minimal disruption of the natural environment [25, 6, 7]. One last advantage is to use a biomimetic approach to learn more about nature by attempting to create a robotic model of specific mechanisms [18, 16].

1.2.2 Applying soft robotics for underwater Robots

Numerous approaches have been developed to replicate biological underwater locomotion as shown in figure 1.1. Four different kinds of actuation are highlighted.

String actuation is arguably the most basic type of actuation performing very simple movements. One connects a string to soft robotics and recognises a deformation upon contracting the string. Inspired from nature one can compare this actuation type with tendons in the human/ animal body. Therefore one can argue, that there is significant potential to realise complex movements utilising multiple carefully designed actuators synergistically. The main problem is how to generate the contraction of the string, where typically a motorised pulley is used. As the force is transmitted over the string it additionally poses significant waterproofing challenges when applying underwater.

Pneumatic actuation is among the most common types of actuation for soft robotics. Underwater, liquid is pumped from one chamber into another resulting in a deformation. Applications are not limited to fish tails [17, 20] , but also include grippers [26, 10] and sea stars [4]. While the actuation has proven to work reliably, primarily thanks to extensive research in this direction the pumps actuation the soft robotics remain the main challenge especially when requiring waterproofing. Robots have been developed replicating the escape behaviour seen with fish in nature. [20] A highly flexible pneumatic tail enables the robot to form an S- shaped tail during the escape motion.

There are also rigid approaches to propel a fish forward. They include a magnet in coil actuation that has been implemented successfully for miniature underwater robots used for swarm simulations [5]. A coil with a magnet in its core is used. Upon applying a current in the coil the magnet experiences a torque according to the magnetic field from the coil. The force scales poorly making this type of actuation only feasible for smaller underwater robots. Additionally the actuator is a complex part made from multiple small 3d printed parts and needs to be glued in order to seal the wire of the coil leaving the shell of the robot. Nevertheless it provides a robust and small actuation method.

To investigate the swimming movement further, robotic replicates of natural fins or whole animals are built. To mimic undulating swimming rigid hinge joints were used [25, 13]. Here, the traveling wave movement of a Angulliform swimming animal was replicated.

Overall most underwater robots consist of a rigid main- body shell housing the electronics to which external fins are attached. Some exceptions consist of multiple compartments, that move relative to each other resulting in a forward propulsion. Other aspects like buyancy, waterproofing, communication, connections and camera/ intelligence vary significantly across implemented underwater robot.

For all of these underwater robots there is a large trade off between functionality and simplicity. While the robot by Katzschmann et al [17] is able to swim up to 18m deep in the ocean, being controlled using an ultrasonic remote it is highly complex and therefore expensive to build. Furthermore, the swimming speed of robotic replicates of fish locomotion are rather slow with about 0.5-1 body length per second compared to natural fish usually swimming at around 10 body length per second [3].

1.3 Concept of the master thesis

The main challenge posed in this thesis is how to achieve simple actuation of the soft fin tail in order to generate a thrust. As shown in the state of the art

of current underwater robots various types of actuation are explored. For string and pneumatic actuation waterproofing poses a significant challenge. This is because the actuator and actuated tail require a physical connection in the form of a string or a pipe translating the force. Multiple compartments connected with hinge joints make a robot inherently complex. While the magnet in coil actuation is a very elegant solution it does not scale well for larger robots and has a complex setup.

A novel actuation method has been invented, verified and implemented to meet the goals set in the beginning of the project. The approach is based on the interaction of an electromagnet and permanent magnet. As the force between the two is translated via the magnetic field they do not need to interact directly. This enables one to place the electromagnet in a closed off waterproof housing while the permanent magnet is out in the water, integrated in the soft tail. This is an inherently reliable and simple setup. Additionally the force between the permanent magnet and electromagnet can be controlled precisely and instantly by adjusting the current through the electromagnet. The main drawbacks of magnetic actuation are the energy efficiency and low power at larger distances.

The actuation method is integrated into a complete autonomous underwater robot. The shape is designed in a humanoid way, taking inspiration from comic characters like a mermaid. In line with most current underwater robots a rigid shell houses the essential electrical components. It represents the main body and head of the character. The soft tail is attached to it propelling the underwater robot forward. Peripherals like hair and arms are shaped like a fin improving the fluid-dynamics during swimming. A camera is included to enable autonomous tracing of objects under water. Electromagnetic wireless communication is used at the surface and out of the water.

Chapter 2

Actuation Method

2.1 Actuation priniciple

As seen in figure 2.1 the actuation idea utilises the simple repelling and attracting force between an electromagnet (EM) and a permanent magnet (PM). The magnetisation of the iron core of the electromagnet is set by applying the corresponding current to the coil, wrapped around it. This results in a negative or positive force between the EM and PM. As no physical connection is necessary to translate the force the electromagnet is placed in a waterproof body housing the electric components. The permanent magnet is placed inside a soft silicone cast tail. By applying a current to the electromagnet the force on the magnet changes. This causes the tail to move accordingly. To create the desired undulating movement two pairs of electromagnets (EM) and permanent magnets (PM) are used.

The successful implementation of the magnetic actuation method was devided into three steps.

- **Magnet electromagnet interaction** First the EM and PM interaction

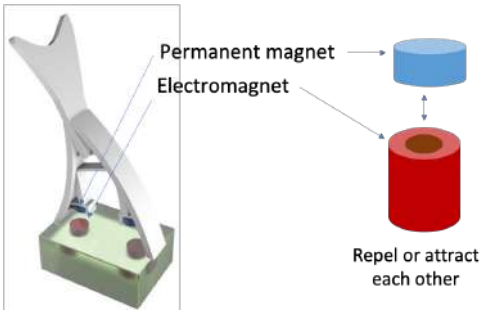

Figure 2.1: The fundamental actuation principle: The attracting and repelling force between the Electromagnet and Magnet causes the soft tail to generate an undulating movement

was investigated to maximise forces and identify the distance between the magnet and the coil, at which significant forces are applied.

- **Soft tail design** The soft silicon cast tail needs to translate the force of the PM to a strong undulating movement.
- **Caudal fin design and control** The undulating movement needs to propel the underwater robot forward with significant thrust. A bioinspired approach is utilised.

2.2 Magnet electromagnet interaction

To optimise the force applied at the respective distance to the permanent magnets two things can be improved. The electromagnet (EM) can generate a stronger magnetic field and the permanent magnet (PM) can have a stronger dipole moment. The dipole moment of a PM can be increased by having a higher remanence magnetisation or a larger volume. The volume is constrained to fit inside the soft tail. The magnet material used is N52 grade neodymium which is one of the strongest magnetic materials commercially available. The rating corresponds to a remanence magnetisation of $B_r = 1.48T$. For the dimension of the used magnet ($r = h = 6.35mm$) the overall magnetisation when considering the whole magnet as a single dipole is $m_m ag = 0.947A \cdot m^2$.

As the PM leaves small room for optimisation the focus is on optimising the electromagnet. The dimensions of the solenoid including width, length and wire diameter need to be chosen. Additionally an iron cylinder with a high permeability is placed at the core of the solenoid focusing the field and therefore increasing the attraction forces.

To calculate the magnetic field of the coil it is considered as an assembly of multiple single current loops. A single current loop results in the following field along its symmetry axis.

$$|\mathbf{H}_{\textbf{single loop}}| = \frac{Ia^2}{2(a^2 + x^2)^{3/2}} = (\frac{I}{2a})(1 + \frac{x^2}{a^2})^{-1.5} \tag{2.1}$$

Here a is the radius of the coil and x is the distance along the symmetry axis from the single coil. I represents the current through the wire. The total magnetic field is the summation over all current loops.

$$|\mathbf{B_{total}}| = \mu \cdot \sum_n \mathbf{H_{single\ loop}} \tag{2.2}$$

$$F_x = m_{mag} \cdot \frac{\delta \mathbf{B_{total}}}{\delta x} \tag{2.3}$$

$$= -m_{mag} \cdot \mu \cdot \sum_n \frac{3Ia^2x}{2(a^2+x^2)^{5/2}} \propto m_{mag} \cdot I \cdot n \cdot x^{-4} \tag{2.4}$$

The resulting force on the permanent magnet with a dipole of m_{mag} in room with permeability μ is evaluated. Along the symmetry axis of the electromagnet the only non zero force is in the x direction. The force scales linearly with the magnetic dipole of the permanent magnet, the current and the amount of current loops n. It drops with the power of four with the distance between PM and EM.

Consequently the current and windings should be maximised. The limitations include heat distribution and power output of the electronics. The resistance of the whole coil wire is important as it determines the resulting current depending on the applied voltage ($I = U/R$). The resistance depends on the total length of the wire and the thickness of the wire (resistance per distance). Using a thicker wire results in a lower resistance increasing the current when applying the same voltage. However the density of the windings is reduced. This affects the overall magnetic field in opposite ways. Therefore a trade off has to be found. The wire used is the 26 AWG Enameled Copper Wire. It has a diameter of 0.4 mm and a maximum resistance of 141.7 Ω/km.

To estimate the magnetic field and resulting forces depending on the parameters a simulation has been written. Based on formula 2.4 single current loops are placed virtually according to the electromagnet dimensions. The sum and derivative in x direction then determine the force applied to the permanent magnet at respective distances x. This enables the immediate estiamtion of When changing the dimensions of the coil the response of the magnetic field can be observed.

The also important influence of permeability μ was simplified in the simulation by assuming vacuum with a permeability of μ_0 scaled by the factor of the effective permeability $\mu = \mu_0 \cdot \mu_{eff}$. As the iron core has low remanence this approximation can be made. However, by utilising a more complex 3D simulation and accounting for remanence time dependencies and the spacial layout of the components could be further optimised.

After considering the stated aspects a coil with a soft iron core of 12.7mm diameter, an outer diameter of 22mm and a length of 32mm was chosen. Its force applied to the permanent magnet is measured and shown in figure 4.1.

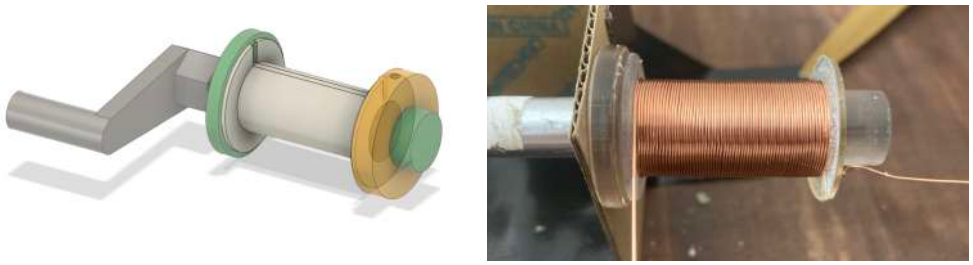

Figure 2.2: Winding of an electromagent using 3d printed guide rails.

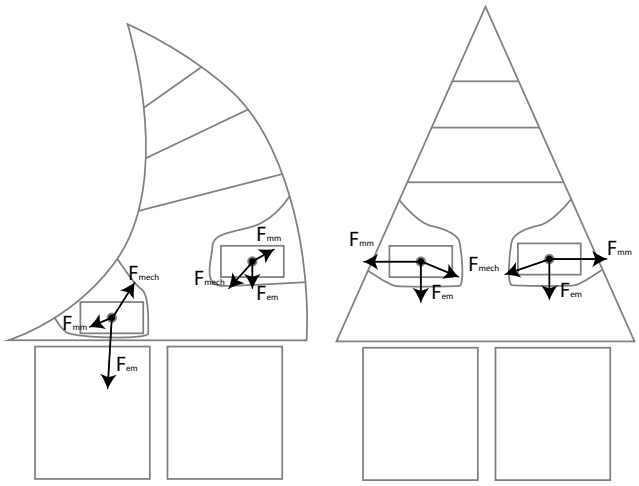

Figure 2.3: Overview of the different forces applied to the magnets. F_{em} describes the interaction between the permanent and electromagnet; F_{mm} describes the interaction between the two permanent magnets; F_{mech} describes the force applied due to the compliant structure and fluid drag.

2.2.1 Fabrication of the electromagnet

To fabricate the the electromagnet 3d printed guide rails have been designed (figure 2.2). A guide is placed in the winding setup shown in the figure. Enameled wire is locked on the guide. One hand rotates the setup consistently and the other hand feeds the wire in the correct place. After fully winding the coil the iron core is placed in the center of the guide and contacts are soldered. The finished electromagnet is then placed in the underwater robot.

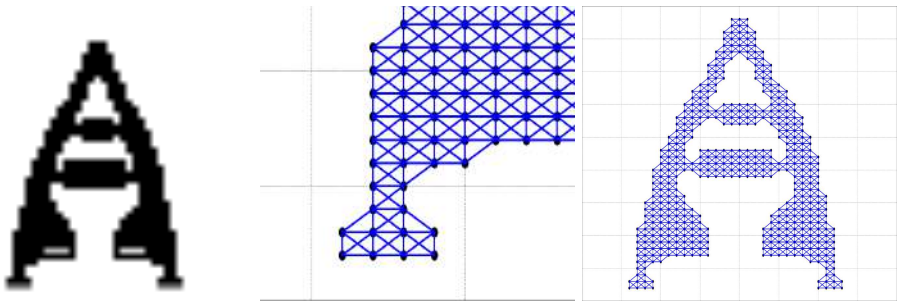

Figure 2.4: Simulation of the compliant tail response: A spring network is used to estimate the behaviour upon experiencing the attractive or repelling force of the magnets.

2.3 Soft tail design

2.3.1 Shape design approach

The main task of the soft tail is to translate the force of the magnets into a flapping tail motion. The overall tail design is originally inspired from triangle shaped passive grippers [8]. Their triangular shaped ladder design causes a bending motion upon a pressure acting on one of its sides (compare figure 2.3. Instead of an outside force causing the bending motion magnets are placed on either side at the bottom of the tail. This allows the permanent magnets to be close to the electromagnets to transmit sufficient force.

As the permanent magnets are the initiators of the tail movement it is important to consider the forces acting on them (figure 2.3). The force between the electromagnet and permanent magnet is most important. It is the only actively controlled force which is achieved by altering the current through the electromagnet. Only if the force dominates over the sum of the all other forces one can detect a movement. Additionally to the controllable magnetic force there is an inherent attraction between the electromagnet and permanent magnet. The two permanent magnets repel each other as they are poled in the same direction. Their interaction can become significant as they get closer, which is noted in the force $F_m m$. Finally there is the mechanical force from the tail acting upon the magnets. It includes the compliance of the silicone structure and the drag in the water.

Based on these initial thoughts the forces are studied individually and prototypes iteratively improved. The findings are documented in the results section.

Various design alternatives were conceptualised. To estimate the compliant response to the force of the magnet a 2d simulation is developed. The approach is based on a spring network. A low res image with marked pixels is used to define the shape of the structure to analyse (compare figure 2.4).

Different brightness values mark rigid areas or areas where forces are applied - eg. the magnets are placed. From those pixels a grid network is determined. Vertical, horizontal and diagonal nodes are connected using a joint. Forces on those joints are iteratively computed and the position adjusted to minimise forces. The underlaying principle is the one of a spring network.

2.3.2 Material choice

Additionally to the shape of the caudal fin the material is also a very important property. There are various types of silicones each having advantages and disadvantages. Please find a table below highlighting silicones that were used/ taken into consideration during prototyping.

Name	**Hardness Shore A**	**Pot life/ cure time**	**Description**
Body Double Silk	25	5min/ 25min	Fast cure time, very skin safe, good for workshops with limited time
Dragon Skin 20	20	25min/ 4h	Very common Silicone, good for prototyping
Smooth Sil 945	45	25min/ 6h	Hardness significantly higher while retaining good stretchability and mechanical properties

More information on the Shore Hardness scale can be found here: https://www.smooth-on.com/page/durometer-shore-hardness-scale/.

While all materials were tested and worked the Smooth Sil 945 was chosen as the ideal one due to its higher hardness making a thinner and more custom tail design possible. A Shore A hardness of 20 is roughly comparable with a rubber band and 45 with that of a pencil eraser.

2.3.3 The fabrication process of the soft silicone tail

Through a iterative process the fabrication of the soft silicone tail has been refined. Originally a traditional 3d printed mold was filled with two component silicone and cured. As the complexity of the structure increased two molds were made and then combined using a second curing step. To achieve maximum flexibility regarding the tail design and to have a precise and repeatable shape injection molding was used. This process is also commonly used in industry due to its convenient workflow, speed and repeatability.

As the name injection molding implies, silicone is injected into a cavity. The most crucial part is to allow the air to escape such that the silicone completely fills each cavity. A proper design of the form is crucial to ensure a successful injection molding process. Therefore I list the most important aspects to keep in mind when designing an injection mold. As a reference find images of my injection mold in figure 2.5.

1. Design the desired shape of the tail
2. Enclose the tail in a larger rectangular box, leaving extra room for screws around the corners. Then substract the component from the rectangular box to recieve the hollow mold.
3. Split the mold to be able to take the silicone part out of the mold after curing. Keep in mind the following things:
    - Do not have overhangs in your final parts. Choose the parting line between objects accordingly. Ideally all vertical walls should be drafted slightly (1-3 degrees).
    - For some designs a two part mold does not suffice. The overall mold then needs to be cut into 3 or more pieces.
    - Make the perimeter of your top and bottom have a drafted lip to ensure self- reliant alignment.
    - Use screws approx. every 15-20mm to secure the mold together. Here cutouts for square nuts (M5) were used to be able to fasten the screws well.
    - Take into consideration, that due to the examined heat when curing the material can shrink and expand. Therefore it is advised to break all corners on the female mold side.
4. Determine a flow concept of the silicone during the injection molding process.
    - The material should be injected at the lowest point of the mold. Here a injection port channel can be used to lead to the appropriate point.
    - Place vent holes at the top part in areas where air gets trapped. They should end at the same height to avoid excessive overflow of material.

The process of injection molding itself after designing the mold is well established in the lab and therfore straight forward. After 3d printing the

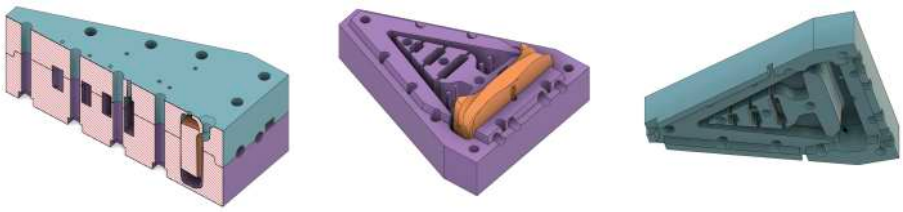

Figure 2.5: Cross section, bottom and top of the injection mold used to cast the soft caudal tail.

mold it is baked in the oven at 65 degrees celsius over night to remove any materials making the silicone stick to the mold or causing cure inhibition. Before injection molding one applies mold release to the individual parts to cover all surfaces. Assemble the mold and fasten all the screws. Then a pressurised system established in the Lab was used to inject a homogenous 1:1 mix of two component silicone in the injection port channel. Here it is important to apply constant pressure through the whole injection molding process to reduce the formation of bubbles. As soon as all the vent holes start leaking silicone one waits for about another 3 seconds and then stops injecting silicone. The mold is then cured according to the package description. To accelerate the process the injected mold is placed in the 65 degree oven. After fully curing the part the mold is taken apart and the finished piece removed.

2.4 Caudal fin design and control

The goal of the whole actuated tail is to create a maximum forward thrust. To achieve this the movement of the tail needs to be translated into a fin stroke. A bioinspired approach is chosen to design the caudal tail. Receiving inspiration from biology makes sense as there are not only millions of examples in nature, but evolution has perfected swimming over billions of years. The optimal shape of the fin is investigated and its control including the amplitude and frequency analysed.

2.4.1 Bio- inspired approach

In nature one separates between Thunniform and Anguilliform swimming. While the latter describes an undulating locomotion in the form of a traveling wave, the former describes an oscillating fin. The two types are compared in the table below:

Thunniform swimming	**Angulliform swimming**
Oscillating fin	Undulating locomotion
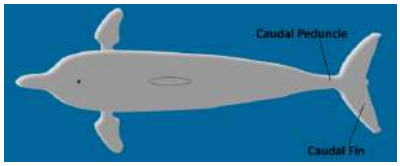	
Example Species: Tuna, Doplphin	Example Species: Eel, Moray
High maximum velocity	High acceleration
Undulating movement confined mostly to the caudal fin Often fin crescent shaped and connected through thin section called caudal peduncle Allows swimming analysis only considering tail	Traveling wave motion through the whole body Body is often uniformly shaped Whole fish needs to be taken into account

In nature usually none of these extremes are present, but a combination of both. For this approach a tail motion similar to thunniform swimming was chosen. It has been extensively studied in nature [24, 11, 28]. While there are some angulliform approaches [13, 25] a flapping tail motion is most common in robotic fish. It can be implemented in a significantly simpler way and provides faster and more efficient propulsion [27, 28].

2.4.2 Theoretical analysis of Thunniform swimming

In figure 2.6 the optimal mechanics of an oscillating fin are described. The body in the water tilted at an angle β is considered. For the left graphic the fin is moving in the direction of propulsion with a speed of v_0 and down due to the flapping motion with a speed of w. This results in a velocity vector U of the water 'hitting' the caudal fin. The interaction results in a Force $F_\perp$ that can be devided in a Forward thrust force F_T and a Force $F_\parallel$ parallel to the velocity vector U. The angle α between the direction of the waterflow and the orientation of the fin determines if there is forward thrust. If $\alpha = 0$ then $F_T = 0$. The figure on the right the illustrates an upward motion.

To generate more thrust, one can increase the vertical flow speed w. This results in a larger magnitude of U and a larger angle α. To increase w one can oscillate the tail with a larger magnitude H or higher frequency f. If w becomes too large however the relation between F_T and $F_\parallel$ is becomes unfavourable. This results in a significantly higher power required with

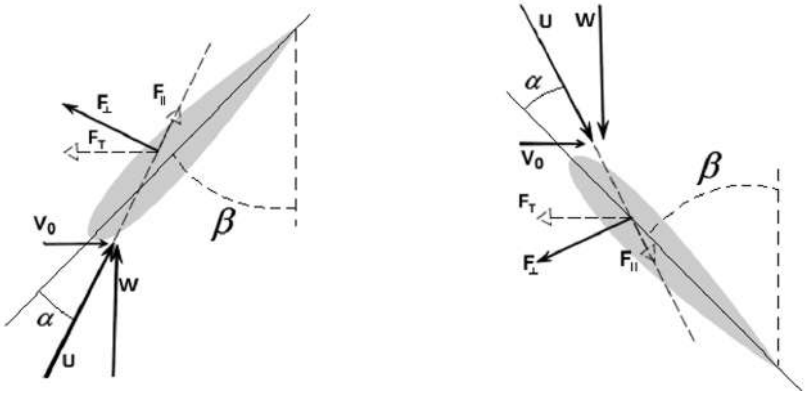

Figure 2.6: Mechanics of Thunniform swimming riding along with the fin as it moves down (left) and up (right). v_0 is the water flow in swimming direction and w the flow from the oscillating movement. Graphics from [1]

negligible thrust increase and therefor leads to lower propulsive efficiency. A benchmark for optimal efficiency that has been determined from robotic fins is:

$$\frac{fH}{V_0} = 0.30 \tag{2.5}$$

f and H are the frequency and Amplitude of the oscillating fin respectively. Fish have optimised the thunniform swimming to achieve a propulsion efficiency of 80-90% when swimming at optimal conditions.

Graphics and text adapted from [1].

2.4.3 Fin shape and material design

The fin is designed with mindset of replicating predominantly thunniform swimming. A custom cut out plastic sheet is used as the fin. It is attached to the soft caudal tail by sliding in a specificially designed notch. There is no glueing required making it quick to interchange different fins.

The fin design is inspired by similar approaches found in literature. Jusufi et al. [16] implemented a pneumatically actuated robotic fish fin using a sheet plastic as the fin. Key features like the frequency, phase, overlap and dead time were investigated and related to the locomotor forces. Additionaly to the general trend of increased thrust from higher frequencies there was also a local maximum observed. The impact of the tail shape and stiffness on swimming speed was tested by Feilich et al. [9]. Here no optimal foil could be found exhibiting highest performance in all metrics. The tail with

an aspect ratio calculated according to 2.6 and a deep peduncle achieved a highest self propelling swimming speed.

$$AspectRatio = \frac{l^2}{A} \tag{2.6}$$

l describes the length of the fin and A the area.

2.5 Tail control

The fin position and motion is determined by the electromagnetic force, which can be controlled by altering the current through the electromagnet. The frequency, amplitude, bias and efficiency are determined by applying the correct forces over time. There is no feedback implemented making this and open loop controller.

Ideally the frequency and amplitude of the osciallting tail movement should be high to increase thrust (compare [16]). The higher the actuating force the larger the amplitude and faster the movement in the desired direction enabling faster frequencies. Therefore maximum currents in opposite directions on the magnets should be used. This makes them synergistically move the tail to one side. One magnet pulling and the other one pushing. A bias can be introduced by introducing a time difference between the two sides during one period. By resting the tail on either side for slightly longer the underwater robot steers in that direction.

The two electromagnets are controlled using the Raspberry Py. Here a Python code is implemented determining the stimulating pattern. It consists of a period T in which the pattern is applied and then repeated. Therefore T determines the frequency $f = 1/T$. One can then determine the current direction and amplitude in 100 sub steps during one phase by setting an array. This allows forward movement by applying opposite currents to both magnets for 50 sub steps and switch for the second half of the period. Biases can be introduced by switching not at 50% but a higher or lower value. The efficiency of the tail however can be greatly improved by only applying maximum currents during moments, where the maximum force is required. This was not tested further, however the software framework is set up to apply arbitrary cyclic inputs.

Chapter 3

Overall Body Design

3.1 The Layout

The soft caudal tail is attached to the main body using a sleeve, which is part of the silicon cast tail. The main body is a waterproof shell housing the electronics including the electromagnets in the very back. These then interact with the soft tail as described in chapter 2. On the Main body modular arms and a head can be attached. These currently passive components

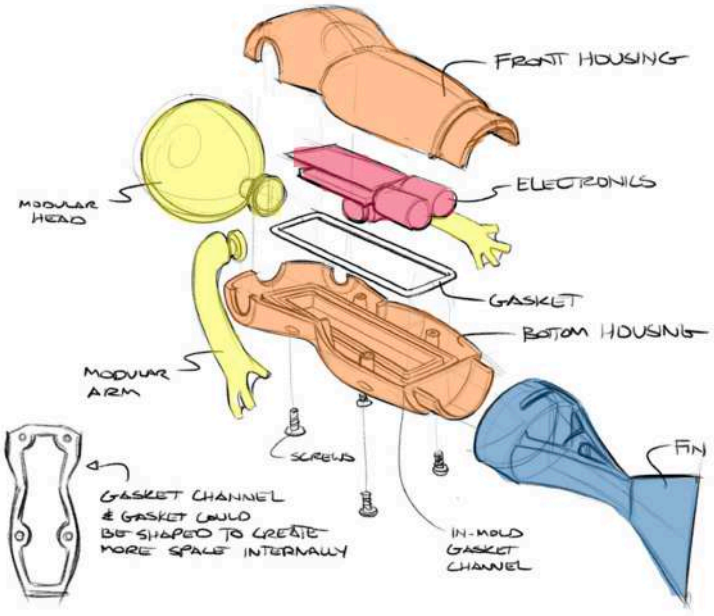

Figure 3.1: Implementation concept. (Orange) Main Body; (Red) Electronics; (Yellow) Extra components; (Blue) Soft silicon cast tail (Sketch by Derek Cascio)

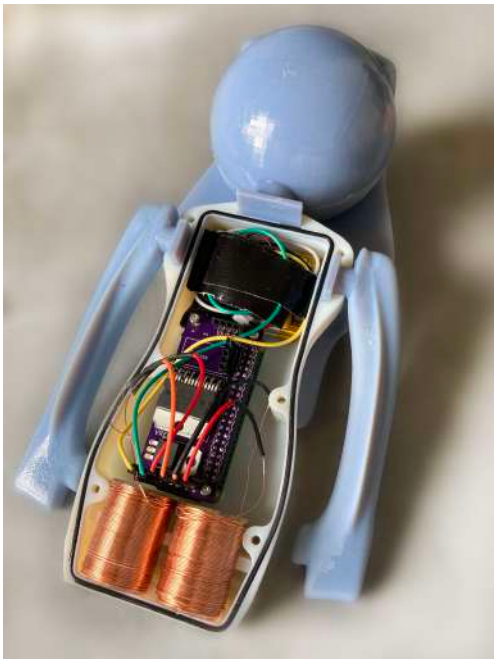

Figure 3.2: The body after removing the top shell. The battery, control boards and electromagnets (top to bottom) are revealed.

contribute to the weight distribution and fluid dynamics.

3.2 Shell Design

The overall body is inspired by a comic style superhero character. Based on initial sketches of a general look a 3d model was elaborated. Additionally to the look constraints, fluid dynamics, fitting the components and weight distribution/ buoyancy has to be considered. The electromagnets are placed in the lowest part of the body touching the wall. This ensures a minimum distance between electromagnets and permanent magnets. The rest of the components are fit in the long main body. Arms and the Hair are designed in a shape, such that their finlike features enhance the fluid dynamics while swimming. This reduces twisting of the main body caused by the flapping fin.

The two part hull is held together with six screws. Square nuts are inserted into the 3d printed design to enable a proper fastening of the M3 screws. A channel around the inner side of the hull is filled with a gasket. Upon fastening the screws the notch from top part of the hull fits directly into the gasket filled channel creating a waterproof seal.

To fit the inside components extra features were implemented. Four screw

Figure 3.3: The CAD model of the underwater robot

sockets for the custom PCB and Raspberry Pi and crescent shaped mounts to place the electromagnets.

The parts were designed in Solidworks Fusion 360 program (CAD model illustrated in figure 3.3). All rigid pieces are 3D printed. Polyjet printers by 'stratasys' with vero blue and white material were predominantly used.

3.3 Weight distribution and buoyancy

The goal is to achieve neutral buoyancy to float steadily at every depth. As there is currently no active buoyancy control implemented the fish is slightly positively buoyant such that the hair of the mermaid slightly sticks out at the surface. This way the rest of the mermaid stays at a constant level under water.

Additionally to the overall buyancy - the difference between weight of the object and weight of the volume of displaced water, the center of these weights are also important. Placing the center of mass significantly below the center of buoyancy ensures the underwater robot is inherently stable in the water. The center of gravity and buoyancy as well as their respective values were compared and the design adjusted. Additionally multiple mounting places for weights are distributed to fine tune the weight distribution. This includes the tip of the hands to ensure a lower center mass.

3.4 Electronics

The overall layout of the electronics is shown in figure 3.4. A Raspberry Pi Zero W was chosen as a digital processor. While being compact in size it offers wireless communication, a camera interface and GPIO (General input output pins) pin control making it a clear choice. To enable the Raspberry

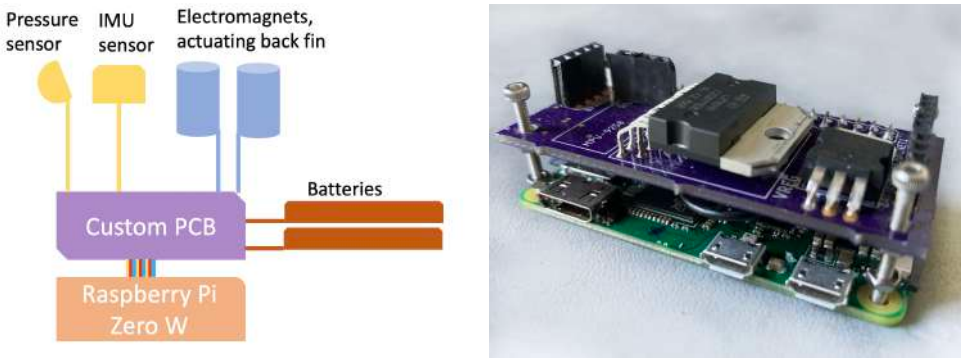

Figure 3.4: (left) Overview of the electronic components and their connection; (right) The custom designed PCB board mounted on the Raspberry pi Zero W

pi to interface with sensors and actuators and receive power a custom board was designed, that is mounted on the Raspberry Pi.

The motor driver chip L298N is the main component of the PCB. It drives the electromagnets using the logic input from the GPIO pins of the Raspberry Pi and the direct power of the battery. It supports currents up to 2A for each electromagnet and Voltages up to 46V, which is notably more that the 1A, 7.4V currently used. To power the logic of the L298N chip and the raspberry pi the voltage regulator L7805 is used. It provides a 5V output current of maximum 1.5A.

Two 3.7V LiPo batteries are connected in series, resulting in a total voltage of 7.4V. Each of them having a capacity of 850mAh. The two batteries can power the electromagnet drawing 1A at 7.4V for 0.85 hours or 51 minutes.

A 9DoF IMU Breakout board and a pressure sensor (TE Connectivity MS5803-02BA) can be added to receive feedback during autonomous swimming. They communicate via I2C with the Raspberry Pi and are mounted on the custom PCB.

3.5 Experimental Methods

3.5.1 Magnetic force measurement

A low force testing system by Instron (6800 Single Column Series) was used to measure the force between the electromagnet and permanent magnet at different distances. To attach the components to the machine at a distance, such that there is no significant magnetic interference from the metal parts of the machine custom 3d printed holders were designed. During the test the distance between the two magnetic components was altered at 5mm/s and the force, time and extension recorded. The data was then processed using

python to determine the magnetic force at the respective distance between the electromagnet and permanent magnet. Three tests with no current, $1A$ and $-1A$ through the electromagnet were taken.

3.5.2 Swimming Test

A prerequisite for successful testing of swimming is to ensure the body can freely float in the water. By using weights to calibrate the body and making it slightly positively buoyant it stays right under the water line.

Multiple tail shapes were cut out and labeled. The robot was tested in calm water. It is placed at one side of the water basin and propels itself forward to achieve a certain swimming speed. The process is video recorded from a top down view (compare figure 4.6). To determine its speed the body length in the video was measured and the time required to surpass this length recorded. By dividing the distance traveled over the time, the velocity is obtained.

Chapter 4

Results and Discussion

4.1 Magnetic interaction

The force on the permanent magnet corresponding to the distance to the electromagnet is measured and compared to the simulated one (figure 4.1). The maximum force is at a maximum if the center of the permanent magnet is at the end of the coil (see Simulated force). It then decreases exponentially as the distance between the EM and PM increases. This is replicated in the experimental tests.

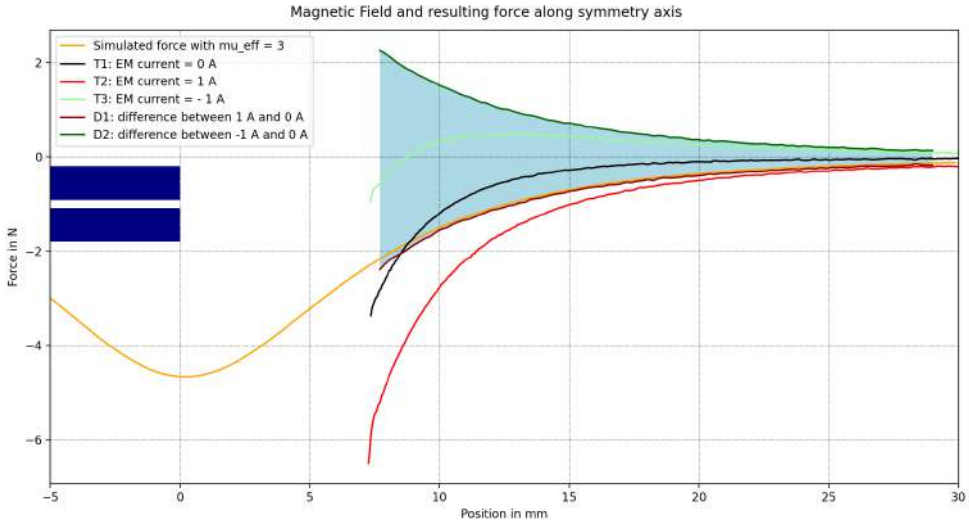

Figure 4.1: The force applied to the permanent magnet depending on its distance to the electromagnet. The response was recorded for 0, 1 and 2 A. The area in blue highlights the total force that can be applied when canceling out the attractive force of the EM and PM with no current applied.

As no current is applied to the electromagnet (T1) one detects an attractive force between the iron core of the electromagnet and the permanent magnet. This force is significantly increased when applying a positive current of 1A. For the inverted current of -1 A the solenoid creates an inverted magnetic field resulting in a repelling force. However a positive repelling force is only observed for distances of 8.5mm and more. As one moves the two components closer, the attractive force between the permanent magnet and iron core outweighs the repulsive force.

For D1 and D2 only the additional force inferred by the current is considered. The attractive force between the permanent magnet and the iron core of the electromagnet is subtracted. The blue area, which spans between D1 and D2 shows the relative force change that can be applied to the permanent magnet depending on its distance to the electromagnet.

From these results we can conclude that the ideal distance to achieve maximum forces is as close as possible. The strong attractive force of the iron core of the electromagnet and permanent magnet at low distances poses challenges though. It exceeds the repulsive forces at -1A below 8.5mm causing the PM and EM to be attracted constantly. This force should ideally be compensated by a compliant mechanical design. One could then apply any absolute force in the blue area to the permanent magnet, enabling both attractive and repulsive forces even at close proximities.

To conclude, the main parameters that can be altered include the position of the permanent magnet while traveling and the compliance of the soft silicon tail. The position has significant impact on the amount of magnetic forces that can be applied. At close distances the compliance of the soft structure needs to compensate for inherent magnetic forces as otherwise no repulsive force can be achieved leaving the tail stuck in one position.

4.2 Tail theoretical evaluation

While the simulation of the tail using a spring network is only a very approximate model it gives an insight into how the structure is going to behave as forces are applied. There were two main use cases of the spring network.

First, established concepts, in particular the ladder shaped triangle inspired by passive grippers [8] is investigated. These already implemented structures are replicated in a pixel drawing and only one parameter changes slightly. In this case the thickness of parts, position of mounting points/ magnets or amount of horizontal connections was varied. Qualitative analysis of the changed response can significantly support the approach of optimising the soft fin tail for e.g. larger deflection. In the first two rows of figure 4.3 the thickness of the ”legs” is increased. As one would expect in-

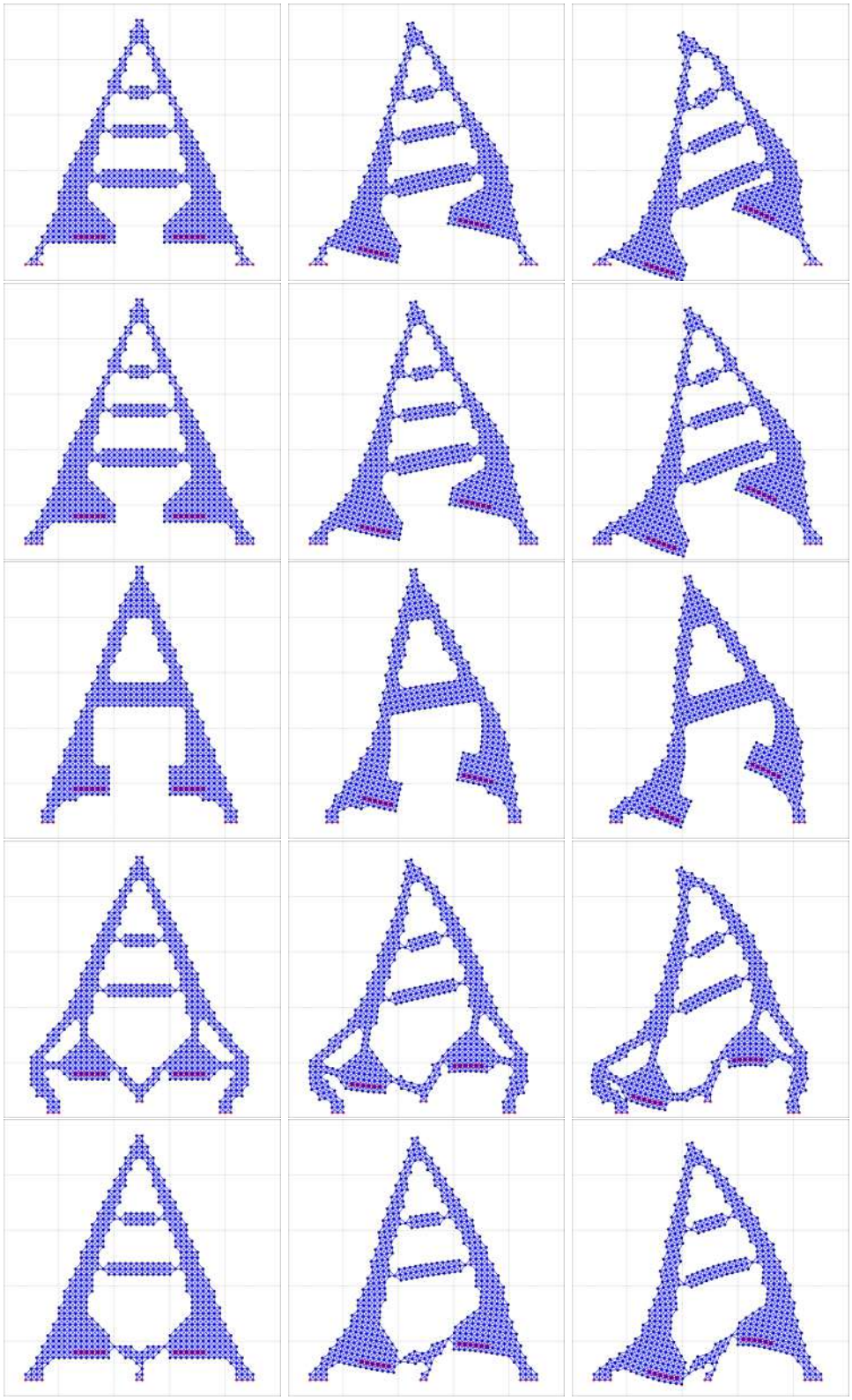

Figure 4.2: Simulating the response of various tail designs to opposite forces applied to the electromagnets. The left column shows the initial state, middle column half force applied and the right one the full force.

tuitively while applying the same force the tail deflects less and the magnet travels further down and towards the middle.

Secondly, a completely new or strongly altered design can be analysed. The qualitative data gives a good indication how the overall body is going to behave. While expecting a certain movement while designing it provides certainty or corrects assumptions significantly faster than the process of manufacturing the soft silicon cast tail.

In row 3 (figure 4.3) a minimalistic structure is analysed. The top triangle stays rigid in itself. The movement of the magnets causes simply the horizontal connection to twist, tilting mentioned triangle. As a fish like bending motion is desired this approach was disregarded.

In row 4 a connection between both magnets is introduced. This restricts the movement of the magnets causing them to stay more horizontal. This improves the force that is applied to the magnets, however the limited movement only results in a slight tilt of the tail.

In the last row the lower mechanism around the magnets is significantly different. Instead of the common in and outward bend of either side caused by the magnets, a vertical translation is observed. This causes an ideal bend of the tip of the tail. However, under close observation the extension of the tail can only be caused under significant movement of the magnets. As the force of the magnets decreases significantly with distance the design requires further refinement.

Overall using such tools is very useful to establish an intuition on how to further improve the design. It can not however be compared to a realistic qualitative simulation nor fabrication of the actual component and testing it.

4.3 Tail actuation

During the process of designing, simulating and implementing various magnetic actuated tails numerous observations and improvements were made. The crucial points that need to be kept in mind when making design choices are summarised below.

- The first and most important step is to determine the initial position and travel of the permanent magnets during motion. Here predominantly the magnetic interactions need to be kept in mind.

  The permanent magnets have to stay within close proximity of the electromagnets to transmit sufficient force (see chapter 4.1). Additionally they should have the same symmetry axis, meaning they are parallel

and have no offset to either side. This ensures that a maximum force from the electromagnets can be applied at given distances.

As both permanent magnets are placed in the same orientation they repel each other. This force can become significant if the magnets are too close. As the magnets pass each other during a tail stroke this force is increasing significantly. This creates a two state system, where the tail is tilted to either side in a low energy state and at a maximum in the middle. This can hinder the actuation of the tail significantly, however could also be exploited. Upon passing the threshold where the two permanent magnets are closest no additional force is required to tilt the tail all the way as the permanent magnets exert that force themselves.

- The soft silicon tail needs to constrain the determined movement of the permanent magnet. Additionally it is ideal to compensate for the intrinsic magnetic forces with the compliant design. For example the magnet magnet interaction can be compensated for by initially placing the magnets close to each other in a relatively stiff design. While the magnets repel each other the soft structure exerts a pushback. If the two forces would ideally compensate each other almost no force would be required to exhibit a tail stroke in vacuum.

  Therefore, the stiffness of the tail needs to be carefully calibrated. Is the structure too hard, barely any movement is recognised. Is the structure too soft the tail experiences uncontrolled movements. Just the right amount of stiffness enables a controlled tail movement. Meaning it constraints the magnets paths and compensates for intrinsic forces.

- Finally, the tail needs to exhibit a significant stroke. Therefore the movement of the magnets needs to be translated into a tail undulating motion. The extension, force and type of deflection are important. Experiencing a bending motion replicates the natural fish movement and can be well translated into significant thrust by attaching a fin.

Overall a tradeoff between range of motion and force needs to be made. As the permanent magnets travel further their force becomes weaker. Translating their movement into a large tail movement also decreases the force of the fin on the water. However, when using a stiff design the tail movement becomes very precise and strong. This tradeoff needs to be well balanced to be able to achieve sufficient frequencies while having a significant amplitude of the tail.

To address these design goals two things can be adjusted: The shape and the material. The shape gives most flexibility and has been investigated using the simulation. Orienting on the Triangle shaped ladder design [8] features like the thickness of the beams and sides were adjusted.

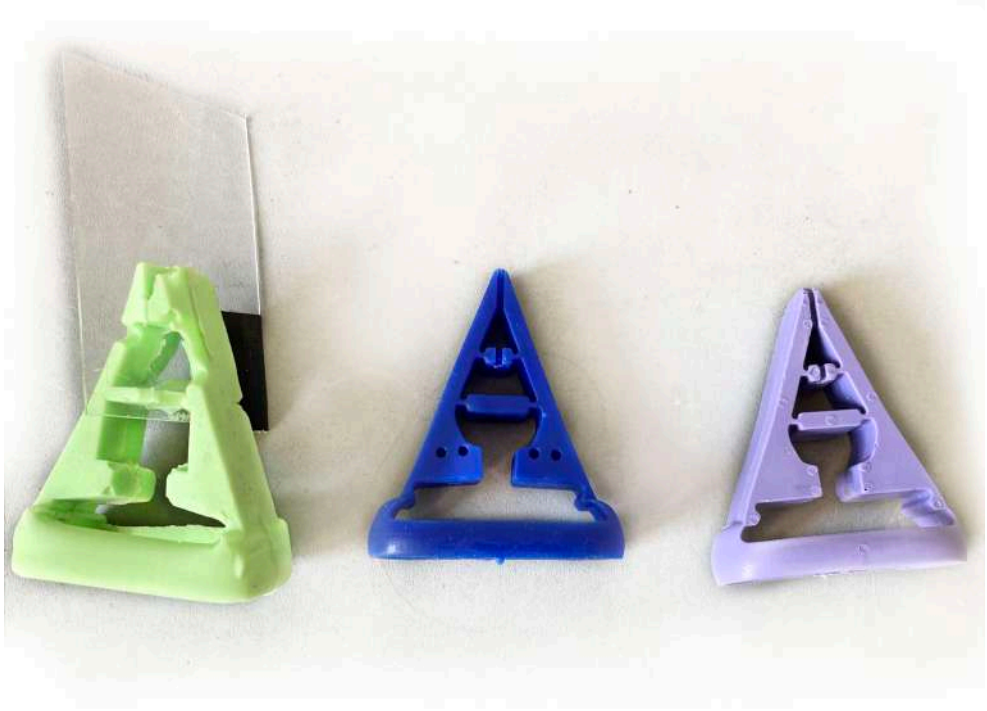

Figure 4.3: Multiple iterations of the tail with increasing hardness from left to right. (left) Body Double Silk; (middle) Dragon Skin 20; (right) Smooth Sil 945

Additionally to the design features of the tail the material choice plays an important role. Multiple materials with various stiffnesses from hardness of approximately a rubber band (20A) to a pencil eraser were used (compare 4.3). Stiffer materials allow for significantly thinner features while retaining rigidity and give therefore more freedom regarding design choices. Additionally the maximum force that can be transfered is higher with stiffer materials. As the material becomes too stiff the force needed to move the tail becomes too high. Therefore a tradeoff has to be found and combined with a corresponding design, that adjusts the thickness of features to have the proper stiffness.

The implemented tail (figure 4.4) features the original Fin Ray inspired design with three horizontal connections. The permanent magnets are placed on the symmetry axis and in close (7.7mm) to the electromagnets. Some niche improvements and features of the implemented tail are highlighted below:

- The two sides are tapered towards the top ensuring a smooth bending motion.

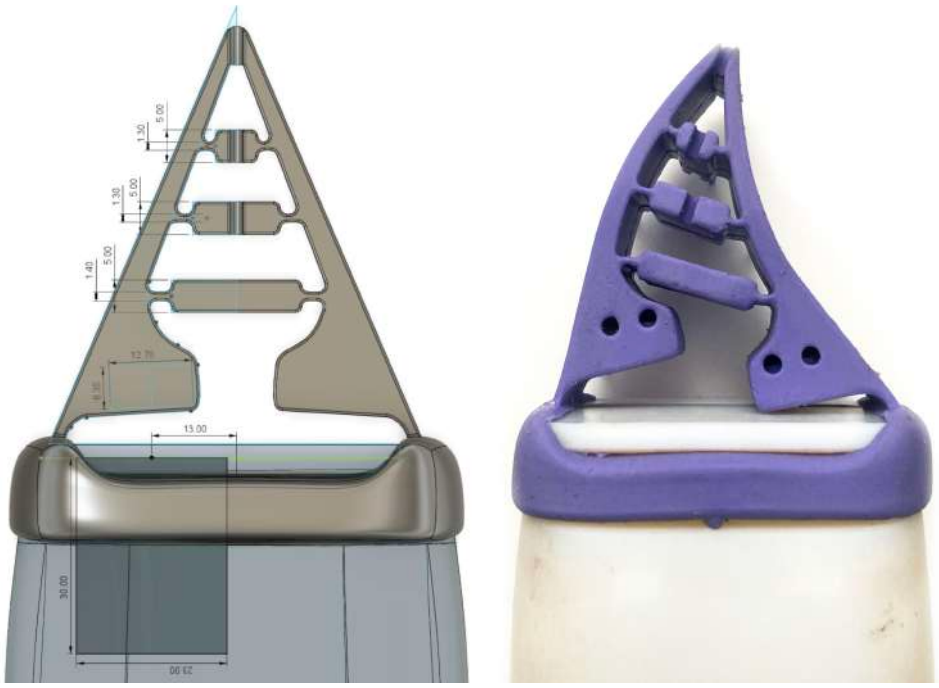

Figure 4.4: The top view of the CAD tail model and real world fabricated tail. Dimensions in mm.

- The horizontal shafts are implemented in a thick way, but use thin connection joints at either end. This reduces friction while retaining their functionality of keeping the right distance to create the bending motion.
- The magnets are embedded with a very thin silicon layer around them. This is enabled by a wire mesh which is embedded in the silicone around the magnets. The chance of the silicon tearing at these high force points becomes significantly less.
- The tail fits perfectly on the mounting ring at the end of the body. This is crucial as even a little bit of play or tolerance of a couple millimetres can have a significant impact on the tails performance.

4.4 Overall Body

Integrating an autonomous underwater robot in a humanoid shape poses significant challenges. Instead using common fish as a template and designing one round main body, the human body is significantly thinner and elongated. Additionally, extremities like the head and arms need to be accounted for. The final design integrates all components in a mermaid char-

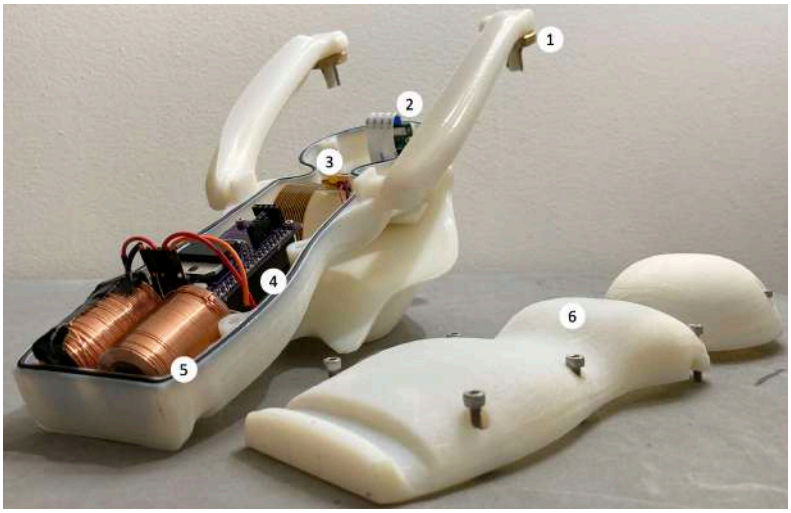

Figure 4.5: The final design with (1) adjustable weights, (2) a front camera, (3) batteries, (4) processing unit, (5) electromagnets, (6) top hull.

acter as seen in figure 4.5. The head is combined with the main body to house the camera in the very front. Having no connections from inside to outside of the main hull enables a simple and effective waterproofing. Additionally it makes the whole setup very flexible and easy to assemble as all parts are screwed together using predesigned mounting points. The modular arms can be detached when opening the enclosure. They include mounts for counterweights to be able to precisely balance the weight distribution and buoyancy. Thanks to the orientation of the arms, the centre of gravity is significantly lower than the centre of buoyancy ensuring a stable position in the water. The detachable hair is shaped to act as a dorsal fin stabilising the fish further while swimming. Overall it is a practical design, enabling autonomous swimming of the robotic mermaid.

The length of the main body from head to the thighs is $230mm$. It has a total volume of $7.8 \cdot 10^5\ mm^3$ including arms and hair. The total weight is around 680g depending on the components.

Waterproofing was tested for 10 hours at 0.5m under water. There was no sign of leakage detected. Additionally all swimming tests were carried out without any leakage. This shows, that at least for low depth the gasket screw combination ensures a waterproof seal.

4.5 Swimming performance

When actuating the tail a steady and controlled swimming is observed. The body does not wiggle at all, which is mainly due to the significant disparity

of body mass to fin. This is also the main reason, why swimming seems inert. The large body mainly stems from the design constraints, requiring a larger housing to fit the necessary components and achieve a good weight distribution.

Multiple tail designs and actuation frequencies are tested and shown in figure **??**. In a dry environment with no water a steady oscillation with a frequency of 9.1 Hz was achieved. Upon placing the robot in the water the thrust generated by the flapping tail moves the robot forward (figure 4.6) . The observed extension and frequency of the tail remains the same. The exception is when the maximum frequency of 9.1 Hz is combined with larger tails (T2, T3, T4). Here one detects a decrease in swimming velocity (see figure 4.7) as the frequency and extension can not be maintained due to increased drag. This results in the tail showing uncontrolled twitching.

When taking these exceptions out of consideration the velocity generally increases as the actuation frequency is increased. This behaviour is expected as due to the higher vertical flow speed of the fin more thrust is generated (see chapter 2.4.2).

The maximum swimming speed does not significantly depend on the Tail shape. All tails achieved a maximum velocity of 10 or almost 10 cm/s. The frequency at which this maximum velocity is reached does change. While for the smallest fin (T5) the maximum frequency achieves the fastest movement the other tails have a maximum velocity at 5 Hz. This is most likely due to skipped beats as the drag becomes too high.

Overall this highlights a maximum speed of 10.8 cm/s with steady swimming. Thanks to the simplicity of exchanging fins and tails it can serve as a platform to perform further in depth tests of shapes, frequencies and undulation movement.

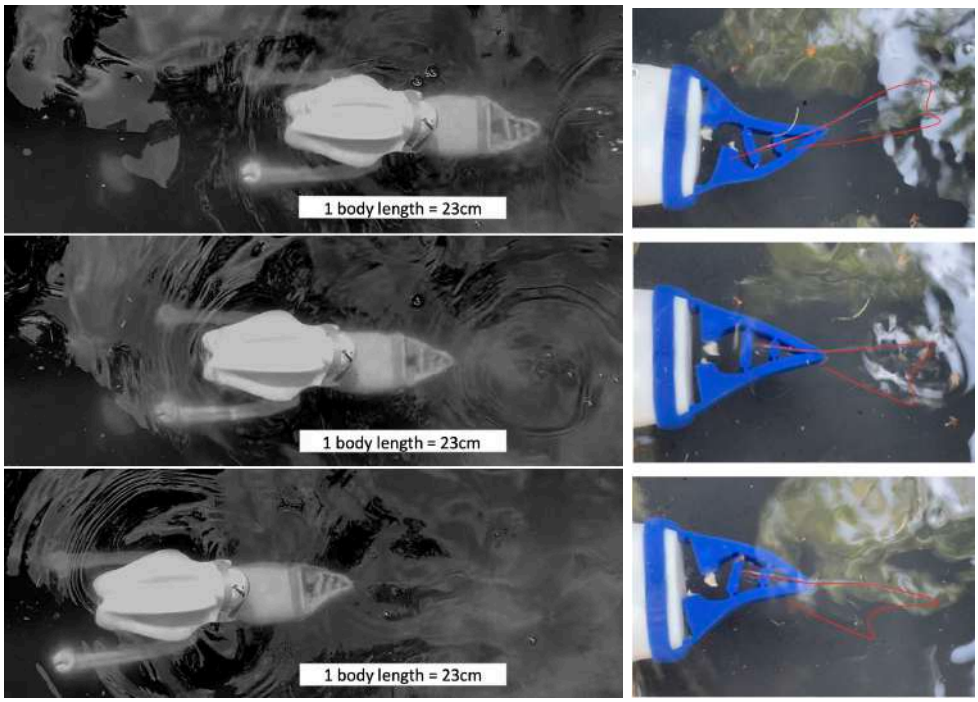

Figure 4.6: (left) Top down view of the mermaid body swimming. (right) Oscillatory behaviour of the fin

Figure 4.7: Comparison of swimming speeds of multiple fin cutouts actuated at various frequencies

Chapter 5

Conclusion

A fundamentally novel actuation method was invented, verified and implemented in an autonomous underwater robot. Starting with requirements and goals a concept was created. It determined the separated two part design of body and tail. One soft and the other one a rigid shell. Next a suitable actuation method was determined, and as no current method fulfilled all requirements a novel actuation method tested. After successfully verifying the basic functionality of the actuation method and fish tail, it was implemented. The overall body and electronics were designed and built and combined with the tail. The whole system was tested of its functionality, its theory investigated and the magnetic force and compliant tail response simulated. Based on the gained knowledge a new iteration was designed and this process repeated.

The final robotic fish combines functionality with a very different human shaped desgin. Rethinking individual components, like creating dorsal fins out of the mermaids hair has enabled such a design. The design is simple, robust and most importantly modular. This is largely thanks to the novel actuation method which enables a straight forward waterproofing and opens up a new possibilities of actuation. Thanks to thoroughly investigating the three main aspects required for a successful actuation autonomous swimming was achieved.

Soft underwater robots have a huge potential that deserves further research. By replicating natural locomotion they can not only be developed to swim fast and efficient but in agreement with nature. This enables applications like scientific marine observation or interaction. A new application scenario considered for this robot is to detect and in the future remove plastic from water. Using image processing and its front facing camera, plastic parts can be detected and traced. These and more applications encourage further research in this fascinating area.

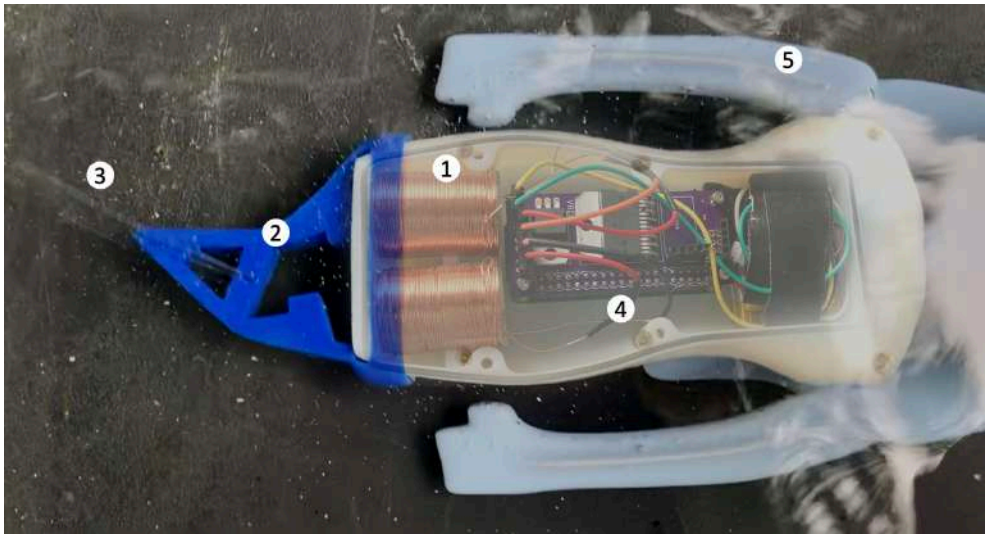

Figure 5.1: The mermaid body, featuring multiple applications for education. (1) Magnetic actuation (2) Soft silicon cast tail fabrication (3) Fin design (4) Software: Controlling the electromagnets and combining with image processing of camera in the future (5) Buoyancy control and weight distribution to achieve stable swimming.

5.1 Applying the underwater robot in education

Thanks to the simple design students are able to assemble the robot themselves in a very modular way. This serves as an excellent platform to learn new skills in soft robotics, electronics, programming and biology. The core learning opportunities are listed below:

- Utilising the novel actuation method of the robot magnetics and its applications can be explained. One could explain the fundamental principles of magnets and then highlight electromagnets. One can then fabricate such an electromagnet and apply it directly in the underwater robot.
- Advanced fabrication of molds can be taught. In industry injection molding is the current standard and it is therefore useful to understand the concept. Additionally students can come up with their own tail designs, which could also be made out of sheet plastic at first. This allows for creative freedom to design an ideal force translation of the magnets.
- Teaching natural fish locomotion and their different fin shapes can find application here too. Inspired by biology [18] one can cut out various fins from sheet plastic and attach them to the tail. This allows one to then test the performance depending on the design of the tail.

- An alternative would be to enable the students to program the underwater robot in a specific way, exploring different behaviours.

5.2 Outlook

The phases of implementation and testing are an iterative process. The next steps that could be taken to further improve the underwater robot are listed below.

- This new actuation method provides various opportunities for further improvements and extensions:
  - To optimise the magnetic force a complete FEM model of the electromagnet and permanent magnet interaction can be developed. This would allow one to add high permeability materials in custom specifically designed places.
  - On top of the current 2d spring network a 3d Finite Element Model of the soft silicone structure can be developed. This would additionally allow for quantitative predictions and optimize the shape for efficient and maximum force translation. Research has shown however, that these predictions tend to be inprecise. A FEM model basted on the SOFA Soft Robotics framework has been attemped.
  - The manufacturing of the silicon cast tail can be adapted such that it becomes possible to build it in a teaching environment. One option would be to provide the finished molds and use a syringe to do the injection molding. Other options would be to go back to a two part mold or enable students to modify the mold as a CAD file or in the real world by adding or removing lego like blocks.
  - A great test for both research and education is to design various fin shapes, cut out of the sheet plastic and compare their effect on speed, efficiency, stability and other parameters.
  - The control of the currents of the electromagnets using software can be refined. While the current method of applying maximum currents achieves maximum amplitude and frequencies alternative approaches could increase efficiency and movement behaviour (eg. have a more slow/ steady/ consistent movement).
- The overall body can be further optimised to improve weight distribution and buoyancy. Additionally an active buoyancy control could be

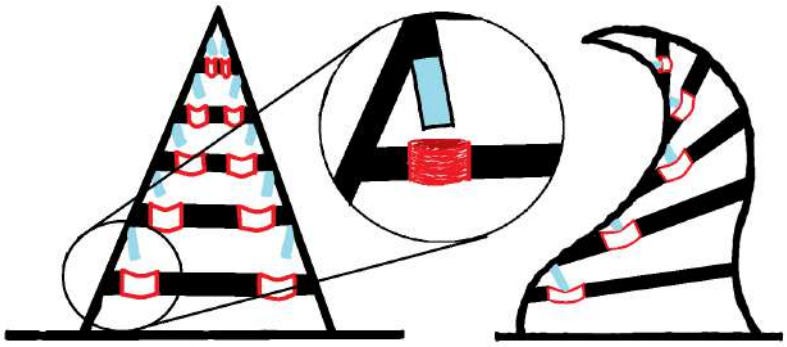

Figure 5.2: An alternative implementation of a soft tail using the same fundamental actuation method. Coils are illustrated in red, permanent magnets in blue and the soft silicon structure in black.

implemented to control the depth of the robotic fish in the water. The following options are proposed:

  - Place a motorised syringe inside the hollow shell with its tip protruding to the outside. The sucked in water from the outside adds additional weight to the body without increasing its volume making the fish decent.

  - Add an actuated dorsal fin (faces up). By designing the body slightly positively buoyant actuating the fin would counteract the positive buoyancy.

  - Actuate the Hair or head of the mermaid to tilt up or down. As the underwater robot swims forward this movement makes it ascent or decent respectively.

- Finally, the addition of a camera, which is implemented in the final prototype enables new possibilties. One option is to combine the control of the permanent magnets with object detection. This allows one to trace an object in the water. Other sensors and actuators could be used in the future to implement additional features. The long term goal of collecting plastic could thus be implemented.

5.2.1 The potential of the novel magnetic actuation principle

The principle of the novel actuation method, utilising attractive and repulsive forces between coils and magnets in a soft environment, has huge potential for other applications. The interaction between coils and magnets has traditionally mostly been limited to cyclic motions and rigid environments e.g. an electro motor. The attractive and repulsive forces were usually not

directly applied due to its strong non linearity and low work range. However, using specifically designed compliant materials like silicone allows for new possibilities. Intrinsic forces can be compensated by the stiffness of the materials, magnetic particles like iron could be implemented inside the soft silicone to guide magnetic fields and advanced structures with e.g. auxetic behaviours designed. A precise simulation of the magnetic forces and interaction with compliant structures is crucial for a successful design. If such a model is developed computational design and fabrication could be applied to build smart structures based on simple inputs.

One idea would be to use multiple small actuators which synergistically actuate complex movements of soft structures. While similar approaches have been tried with pneumatic or string actuated soft robotics [21] they are limited by the complexity of the single actuator, requiring e.g. multiple pneumatic pumps, tubes and cavities. Electromagnets on the other hand transmit their forces via Magnetic fields requiring no physical interaction with the permanent magnet. Additionally it is easy to control and connect many electromagnets using simple circuits as they only need two electrical connections and act like a basic resistors when applying a current for low frequencies.

As an example this could be applied to the discussed fish tail problem as seen in figure 5.2. Multiple small coils and permanent magnets each contract and expand depending on the current applied. This interaction would lead to a strong overall tail bend. Each magnet is only required to excerpt a low force, but due to them working synergistically the overall force and movement is expected to be high.

The overall principle can be compared to the natural bone and skin structure of most mammals. Placing magnetic actuation at the core of soft structures can make them come alive.

Appendix A

Magnetic Theory

A basic overview of magnetic theory fundamentals was established to investigate the interaction between the permanent magnet and electromagnet of the soft underwater robot.

A.1 Fundamental Theory

A.1.1 Constants and Units

Name	Unit	Value	Description
μ_0	$N \cdot A^{-2}$	$4\pi 10^{-7}$	Permeability (degree of magnetisation in response to a magnetic field
B	T — $\frac{N}{A \cdot m}$	$\mathbf{B} = \mu \cdot \mathbf{H}$	Magnetic induction/ flux density
H	A/m		Magnetic field
m	$A \cdot m^2$ — $\frac{N \cdot m}{T}$ — $\frac{J}{T}$	$\mathbf{m} = \int \int \int \mathbf{M} dV$	magnetic moment
M	$\frac{A}{m}$	$\mathbf{M} = \frac{\delta \mathbf{m}}{\delta V}$	Magnetisation

A.1.2 Operators

Nabla Operator/ Gradient: Assume f is a scalar function. Applying the nabla operator to f results in the derivative in all three dimensions on the respective axis. Magnitude of the gradient is the value of its steepest slope.

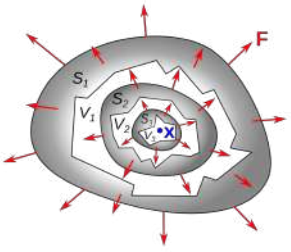

Figure A.1: The divergence at a point x is the limit of the ratio of the flux Φ through the surface Si (red arrows) to the volume $|V_i|$ for any sequence of closed regions V1, V2, V3... enclosing x that approaches zero volume: $div\mathbf{F} = \lim_{|V_i|\to 0} \frac{\Phi(S_i)}{|V_i|}$

$$grad\, f = \nabla f = \begin{pmatrix} \frac{\delta}{\delta x} \\ \frac{\delta}{\delta y} \\ \frac{\delta}{\delta z} \end{pmatrix} f \tag{A.1}$$

Divergence: Scalar product between the nabla operator and and a vector function V. Describes the quantity of the vector field's source at each point. More technically, the divergence represents the volume density of the outward flux of a vector field from a volume around a given point.

Measure of the net flow in and out of a bounded surface; Caused by sinks and sources within the volume bounded by the surface; Calculated by integrating the vector field over the **surface**.

$$div\, \mathbf{V} = \nabla \cdot \mathbf{V} = \frac{\delta}{\delta x} V_x + \frac{\delta}{\delta y} V_y + \frac{\delta}{\delta z} V_z \tag{A.2}$$

Curl of a vector field: Vector product (Kreuzprodukt) between the nabla operator and a vector function V. Describes the rotation of a vector field at a certain location. Calculated by integrating the field along a closed **line**

$$rot\, \mathbf{V} = \nabla \times \mathbf{V} = \begin{pmatrix} \frac{\delta}{\delta x} \\ \frac{\delta}{\delta y} \\ \frac{\delta}{\delta z} \end{pmatrix} \times \begin{pmatrix} V_x \\ V_y \\ V_z \end{pmatrix} = \begin{pmatrix} \frac{\delta}{\delta y} V_z - \frac{\delta}{\delta z} V_y \\ \frac{\delta}{\delta z} V_x - \frac{\delta}{\delta x} V_z \\ \frac{\delta}{\delta x} V_y - \frac{\delta}{\delta y} V_x \end{pmatrix} \tag{A.3}$$

Combination: Combining multiple operators results in:

$$laplace\ operator : \Delta f = \nabla^2 f = \nabla \cdot \nabla f \tag{A.4}$$

$$div(rot\, \mathbf{V}) = \nabla \cdot (\nabla \times \mathbf{V}) = 0 \tag{A.5}$$

$$rot(grad\, f) = \nabla \times (\nabla f) = 0 \tag{A.6}$$

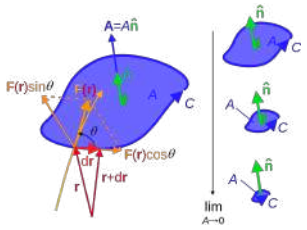

Figure A.2: The components of F at position r, normal and tangent to a closed curve C in a plane, enclosing a planar vector area $(\nabla \times \mathbf{F})(p) \cdot \hat{\mathbf{n}} \stackrel{\text{def}}{=} \lim_{A \to 0} \left(\frac{1}{|A|} \oint_C \mathbf{F} \cdot d\mathbf{r} \right)$.

A.1.3 The Maxwell Equations

The four Maxwell Equations in differential form:

$$\nabla \cdot E = \frac{\rho}{\varepsilon_0} \tag{A.7}$$

$$\nabla \cdot H = 0 \tag{A.8}$$

$$\nabla \times E = \frac{\delta B}{\delta t} \tag{A.9}$$

$$\nabla \times H = \frac{\delta D}{\delta t} + J \tag{A.10}$$

The four Maxwell Equations in integral form:

$$\int E \, da = \frac{Q}{\varepsilon 0} \tag{A.11}$$

$$\int H \, da = 0 \tag{A.12}$$

$$\int E \, dl = \int \frac{\delta B}{\delta t} da \tag{A.13}$$

$$\int H \, dl = \int (\frac{\delta D}{\delta t} + J) da \tag{A.14}$$

A.1.4 Models of B and H relation

B is a measure of how a material reacts to a magnetic field H. (H does not depend on a medium, where as B does). B is the magnetic induction or flux density (in T) in a medium with permeability $\mu(inN/A^2 orhenry/morTm/A)$ or magnetisation **M**.

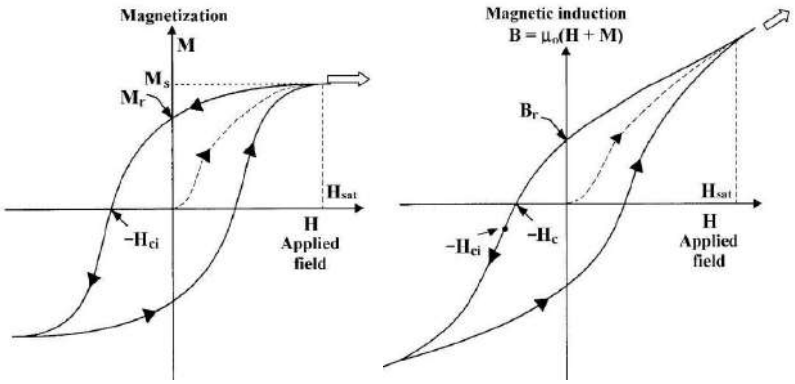

Figure A.3: M-H and B-H hysteresis curves

$$\mathbf{B} = \mu\mathbf{H} \tag{A.15}$$
$$= \mu_0(\mathbf{H} + \mathbf{M}) \tag{A.16}$$
$$\tag{A.17}$$

The permeability μ describes the degree of magnetisation that a material obtains in response to an applied magnetic field. In the general case it is a 3 Dimensional tensor. **M** is the Magnetisation (vector field like **B** and **H**). The magnetisation is defined using the magnetic **susceptibility** χ.

$$\mathbf{M} = \chi\mathbf{H} \tag{A.18}$$
$$\mathbf{B} = \mu_0(\mathbf{H} + \mathbf{M}) \tag{A.19}$$
$$= \mu_0\mathbf{H} + \mu_0\chi\mathbf{H} \tag{A.20}$$
$$= \mu_0(1 + \chi)\mathbf{H} \tag{A.21}$$
$$= \mu\mathbf{H} \tag{A.22}$$
$$\Rightarrow \chi = \frac{\mu}{\mu_0} - 1 \tag{A.23}$$

In hard magnetic materials Once saturation magnetisation is reached **M** is independent of **H** and stays at $\mathbf{M_s}$! The remanence is $\mathbf{B_r} = \mu_0\mathbf{M}$ and describes the Magnetisation under no external field (high for permanent magnets).

For linear and isotropic materials. In soft magnetic materials usually approximately for a certain range (until $\mathbf{M_{sat}}$ / $\mathbf{H_{sat}}$ is reached). We can then approximate eq. A.23 by using μ_r.

$$\chi = \mu_r - 1 \tag{A.24}$$
$$\mu = \mu_0 \mu_r = 4\pi \cdot 10^{-7} Tm/A \cdot \mu_r \tag{A.25}$$

μ_r is the relative permeability: For ferromagnetic $\mu_r \gg 10$; Vacuum/ air $\mu_r = 1$; Diamagnetic $\mu_r < 1$; paramagnetic $\mu_r = 1..10$;

For example, inside iron we have $\mathbf{B} = \mu_0 \mu_r \mathbf{H}$,with $\mu_r = 1000$. This means for a for a given $\mathbf{H}$, iron concentrates the flux lines by a factor of 1000 better than vacuum/ air. Only valid for sufficiently low $H < H_s at$. Otherwise material is saturated.

A.2 From a source to a Magnetic field

A.2.1 Magnetic Vector Potential

The magnetic field can also be described by the vector potential $\mathbf{A}$.

A.2.2 A current through a wire

Assuming constant current, therefore no time dependencies, we can leave out derivations towards time. This gives us the simplified Maxwell formular from eq. A.10:

$$\nabla \times H = J \tag{A.26}$$

From this we can look at the **Biot- Sarvart Law**, determining the magnetic field H generated by an electrical current. First formula determining the contribution $\delta\mathbf{H}$ of a part of a wire $\delta\mathbf{l}$ with a current i. The second formula integrates over the volume of the wire/ object current.

$$\delta\mathbf{H} = \frac{1}{4\pi|\mathbf{r}|^3} i\delta\mathbf{l} \times \mathbf{r} \tag{A.27}$$
$$\mathbf{H} = \frac{1}{4\pi} \int_V \frac{\mathbf{i} \times \mathbf{r}}{|\mathbf{r}|^3} dV \tag{A.28}$$

A.2.3 A solenoid

Applying the Biot Sarvart Law for a single loop results in the following field along the symmetry axis:

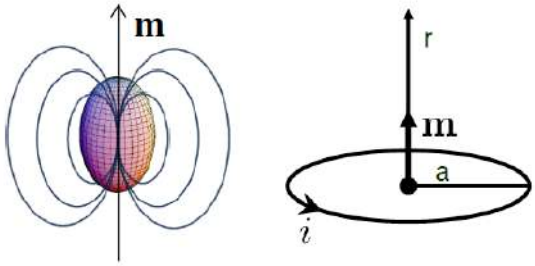

Figure A.4: Illustrations of a dipole

$$|\mathbf{H}| = \frac{ia^2}{2(a^2+x^2)^{3/2}} = (\frac{i}{2a})(1+\frac{x^2}{a^2})^{-1.5} \tag{A.29}$$

y is the radius of the coil and x is the distance along the symmetry axis from the coil. Multiply formula by N to take multiple coils into account. When looking at the field along longer solenoid one receives the following fomula for solenoids of length L and Diameter D.

$$|\mathbf{H}| = (\frac{Ni}{L})(\frac{L+2x}{2(D^2+(L+2x)^2)^{1/2}} + \frac{L-2x}{2(D^2+(L-2x)^2)^{1/2}}) \tag{A.30}$$

Adding a **Magnetic core**. The H field of the solenoid causes the domains inside the core to align in parallel. The magnetic fields add to the wires field creating a large magnetic field. Finally if all domains align, one has reached saturation, where no stronger magnetisation can be reached.

A.2.4 A magnetic dipole

There are two main descriptions for a dipole: A current loop and a linear/ point dipole. Determining the dipole magnitude from a current loop with current i, radius a and Surface area S is described in the first formula. Alternatively one can say a permanent magnet is made by elementary atomic magnetic dipoles. The superposition method supposes that in the elementary volume δV_0, given by position vector $\mathbf{r}_0$, there is a dipole with an elementary moment.

$$|\mathbf{m}| = i \cdot S = i \cdot \pi a^2 \tag{A.31}$$

$$\mathbf{m} = \mathbf{M}(\mathbf{r}_0)\delta V \tag{A.32}$$

The field around it can then be described based on this **magnetic moment m**.

$$\mathbf{H} = \frac{1}{4\pi|\mathbf{P}|^3}\left(\frac{3(\mathbf{m}\cdot\mathbf{P})\mathbf{P}}{|\mathbf{P}|^2} - m\right) \tag{A.33}$$

A.2.5 Magnetic Fields of permanent Magnets

For A cylinder of Length L, radius r the field in axis of distance x from the surface is:

$$\mathbf{B_x} = \frac{B_r}{2}\left(\frac{x+L}{\sqrt{r^2+(x+L)^2}} - \frac{x}{\sqrt{r^2+x+^2}}\right) \tag{A.34}$$

A.3 Forces and torques

In general a force can be calculated by taking the derivative of the energy with respect to its spacial coordinates.

$$F_k = \frac{\delta W_e m}{\delta x_k} \tag{A.35}$$

The fundamental formulas of force applied to an object is:

$$F = \mu_0 \int_v (\mathbf{M}\cdot\nabla)\mathbf{H} dv \tag{A.36}$$

$$\tau = \mu_0 \int_v (\mathbf{M}\times\mathbf{H}) dv \tag{A.37}$$

Applying this formula in a stepwise way:

$$\delta F = \mu_0 v(\mathbf{M}\cdot\nabla)\mathbf{H} \tag{A.38}$$

$$\delta\tau = \mu_0 \delta v(\mathbf{M}\times\mathbf{H}) \tag{A.39}$$

Assuming there is no current flowing in the body (J=0), and using $\nabla\times\mathbf{H} = 0$ we get:

$$\delta F = \mu_0 \delta v \begin{pmatrix} \mathbf{M}\cdot\frac{\delta\mathbf{H}}{\delta x} \\ \mathbf{M}\cdot\frac{\delta\mathbf{H}}{\delta y} \\ \mathbf{M}\cdot\frac{\delta\mathbf{H}}{\delta z} \end{pmatrix} \tag{A.40}$$

Notable is that the force depends only on the spacial derivative of **H** and not its magnitude and a maximum is achieved when **M** and the derivative of **H** are aligned.

A.4 Specific appliation

A.4.1 Permanent magnet grades

Permanent magnets are described using a grade N. Here follows an overview of their properties. The Magentisation is calculated from the remenance flux density $\mathbf{M} = \mathbf{B_r}/\mu_0$.

Official Strength	Residual Flux Density Br [T]	Magnetisation $[\frac{A}{m}]$
N42	1.32	$1050 \cdot 10^3$
N48	1.42	$1130 \cdot 10^3$
N50	1.45	$1153 \cdot 10^3$
N52	1.48	$1177 \cdot 10^3$

A.4.2 Magnetisation of Iron core by the Solenoid

Using a simple two step approach to calculating the Magnetisation/ Magnetic field in the iron core of the solenoid. Using eq. A.30 that defines the field in the solenoid and then determining its Magnetic Flux Density by taking the core Material into account. As iron can be approximated as a linear isotropic material for H fields below H_{sat} we can make use of eq. A.24. Here the magnetic susceptibility or relative permeability of the material is required.

$$|\mathbf{H}| = (\frac{Ni}{L})(\frac{L+2x}{2(D^2+(L+2x)^2)^{1/2}} + \frac{L-2x}{2(D^2+(L-2x)^2)^{1/2}}) \tag{A.41}$$

$$\mathbf{B} = \mu_0 \mu_{eff} |\mathbf{H}| \tag{A.42}$$

$$\tag{A.43}$$

Take effective permeability into account: https://en.wikipedia.org/wiki/Solenoid

Material Description	Relative permeability]
Iron (0.2 impurity)	5000
Iron (rough description of Core bought)	50 000
Purified iron	200 000

Utilising the data from this we can determine the Flux Density (B- Field) for different coils and materials.

Bibliography

[1] Undulatory swimming. *https://s2.smu.edu/propulsion/Pages/undulatory.htm*.

[2] Gunjan Agarwal, Nicolas Besuchet, Basile Audergon, and Jamie Paik. Stretchable Materials for Robust Soft Actuators towards Assistive Wearable Devices. *Scientific Reports*, 6(September):1–8, 2016.

[3] B Y Richard Bainbridge. The Speed of Swimming of Fish as Related to Size and to the Frequency and Amplitude of the Tail Beat. *Journal of Experimental Biology*, 35(1):109–133, 1958.

[4] Michael A. Bell, Isabella Pestovski, William Scott, Kitty Kumar, Mohammad K. Jawed, Derek A. Paley, Carmel Majidi, James C. Weaver, and Robert J. Wood. Echinoderm-Inspired Tube Feet for Robust Robot Locomotion and Adhesion. *IEEE Robotics and Automation Letters*, 3(3):2222–2228, 2018.

[5] Florian Berlinger, Jeff Dusek, Melvin Gauci, and Radhika Nagpal. Robust Maneuverability of a Miniature, Low-Cost Underwater Robot Using Multiple Fin Actuation. *IEEE Robotics and Automation Letters*, 3(1):140–147, 2018.

[6] Richard James Clapham and Huosheng Hu. ISplash-I: High performance swimming motion of a carangiform robotic fish with full-body coordination. *Proceedings - IEEE International Conference on Robotics and Automation*, (iii):322–327, 2014.

[7] Richard James Clapham and Huosheng Hu. iSplash: realizing fast Carangiform swimming to outperform a real fish. *Springer Tracts in Mechanical Engineering*, 12:193–218, 2015.

[8] Whitney Crooks, Gabrielle Vukasin, Maeve O'Sullivan, William Messner, and Chris Rogers. Fin Ray® effect inspired soft robotic grip-

per: From the robosoft grand challenge toward optimization. *Frontiers Robotics AI*, 3(NOV):1–9, 2016.

[9] Kara L. Feilich and George V. Lauder. Passive mechanical models of fish caudal fins: Effects of shape and stiffness on self-propulsion. *Bioinspiration and Biomimetics*, 10(3), 2015.

[10] Kevin C. Galloway, Kaitlyn P. Becker, Brennan Phillips, Jordan Kirby, Stephen Licht, Dan Tchernov, Robert J. Wood, and David F. Gruber. Soft Robotic Grippers for Biological Sampling on Deep Reefs. *Soft Robotics*, 3(1):23–33, mar 2016.

[11] James Gray. The movement of fish with special reference to the eel. *Journal of Experimental Biology*, 10(3):88–104, 1933.

[12] Bianca S. Homberg, Robert K. Katzschmann, Mehmet R. Dogar, and Daniela Rus. Haptic identification of objects using a modular soft robotic gripper. *IEEE International Conference on Intelligent Robots and Systems*, 2015-Decem:1698–1705, 2015.

[13] Auke Jan Ijspeert, Alessandro Crespi, Dimitri Ryczko, and Jean Marie Cabelguen. From swimming to walking with a salamander robot driven by a spinal cord model. *Science*, 315(5817):1416–1420, 2007.

[14] Noah T. Jafferis, E. Farrell Helbling, Michael Karpelson, and Robert J. Wood. Untethered flight of an insect-sized flapping-wing microscale aerial vehicle. *Nature*, 570(7762):491–495, 2019.

[15] Xiaobin Ji, Xinchang Liu, Vito Cacucciolo, Matthias Imboden, Yoan Civet, Alae El Haitami, Sophie Cantin, Yves Perriard, and Herbert Shea. An autonomous untethered fast soft robotic insect driven by low-voltage dielectric elastomer actuators. *Science Robotics*, 4(37), 2019.

[16] Ardian Jusufi, Daniel M. Vogt, Robert J. Wood, and George V. Lauder. Undulatory Swimming Performance and Body Stiffness Modulation in a Soft Robotic Fish-Inspired Physical Model. *Soft robotics*, 4(3):202–210, 2017.

[17] Robert K. Katzschmann, Joseph DelPreto, Robert MacCurdy, and Daniela Rus. Exploration of underwater life with an acoustically controlled soft robotic fish. *Science Robotics*, 3(16):eaar3449, 2018.

[18] George V. Lauder, Erik J. Anderson, James Tangorra, and Peter G.A. Madden. Fish biorobotics: Kinematics and hydrodynamics of self-propulsion. *Journal of Experimental Biology*, 210(16):2767–2780, 2007.

[19] Shuguang Li, Robert Katzschmann, and Daniela Rus. A soft cube capable of controllable continuous jumping. *IEEE International Conference on Intelligent Robots and Systems*, 2015-Decem:1712–1717, 2015.

[20] Andrew D. Marchese, Cagdas D. Onal, and Daniela Rus. Autonomous Soft Robotic Fish Capable of Escape Maneuvers Using Fluidic Elastomer Actuators. *Soft Robotics*, 1(1):75–87, 2014.

[21] Ellen T. Roche, Robert Wohlfarth, Johannes T.B. Overvelde, Nikolay V. Vasilyev, Frank A. Pigula, David J. Mooney, Katia Bertoldi, and Conor J. Walsh. A bioinspired soft actuated material. *Advanced Materials*, 26(8):1200–1206, 2014.

[22] Daniela Rus and Michael T. Tolley. Design, fabrication and control of soft robots. *Nature*, 521(7553):467–475, 2015.

[23] Vanessa Sanchez, Christopher J. Payne, Daniel J. Preston, Jonathan T. Alvarez, James C. Weaver, Asli T. Atalay, Mustafa Boyvat, Daniel M. Vogt, Robert J. Wood, George M. Whitesides, and Conor J. Walsh. Smart Thermally Actuating Textiles. *Advanced Materials Technologies*, 2000383:1–10, 2020.

[24] Robert E. Shadwick and Douglas A. Syme. Thunniform swimming: Muscle dynamics and mechanical power production of aerobic fibres in yellowfin tuna (Thunnus albacares). *Journal of Experimental Biology*, 211(10):1603–1611, 2008.

[25] Katerina Soltan, Jamie O'Brien, Jeff Dusek, Florian Berlinger, and Radhika Nagpal. Biomimetic Actuation Method for a Miniature, Low-Cost Multi-jointed Robotic Fish. *OCEANS 2018 MTS/IEEE Charleston, OCEAN 2018*, pages 1–9, 2019.

[26] Clark B. Teeple, Theodore N. Koutros, Moritz A. Graule, and Robert J. Wood. Multi-segment soft robotic fingers enable robust precision grasping. *International Journal of Robotics Research*, pages 1–21, 2020.

[27] L. Wen, T. M. Wang, G. H. Wu, and J. H. Liang. Hydrodynamic investigation of a self-propelled robotic fish based on a force-feedback control method. *Bioinspiration and Biomimetics*, 7(3), 2012.

[28] J. Zhu, C. White, D. K. Wainwright, V. Di Santo, G. V. Lauder, and H. Bart-Smith. Tuna robotics: A high-frequency experimental platform exploring the performance space of swimming fishes. *Science Robotics*, 4(34), 2019.

Eidgenössische Technische Hochschule Zürich
Swiss Federal Institute of Technology Zurich

Declaration of originality

The signed declaration of originality is a component of every semester paper, Bachelor's thesis, Master's thesis and any other degree paper undertaken during the course of studies, including the respective electronic versions.

Lecturers may also require a declaration of originality for other written papers compiled for their courses.

I hereby confirm that I am the sole author of the written work here enclosed and that I have compiled it in my own words. Parts excepted are corrections of form and content by the supervisor.

Title of work (in block letters):

Development and Evaluation of a soft underwater Robot

Authored by (in block letters):

For papers written by groups the names of all authors are required.

Name(s):	**First name(s):**
Hennig	Robert

With my signature I confirm that

- I have committed none of the forms of plagiarism described in the 'Citation etiquette' information sheet.
- I have documented all methods, data and processes truthfully.
- I have not manipulated any data.
- I have mentioned all persons who were significant facilitators of the work.

I am aware that the work may be screened electronically for plagiarism.

Place, date	**Signature(s)**
Cambridge, MA	

For papers written by groups the names of all authors are required. Their signatures collectively guarantee the entire content of the written paper.